Air-Sea Fluxes in the Western Tropical Atlantic

Lindsay Hogan
Advisor: Professor Ronald Smith
Second Reader: Professor Alexey Fedorov
April 29, 2020

A Senior Essay presented to the faculty of the Department of Geology and Geophysics, Yale University, in partial fulfillment of the Bachelor's Degree.

Air-Sea Fluxes in the Western Tropical Atlantic

Lindsay Hogan

Abstract

At the air-sea interface, vertical fluxes of latent heat, sensible heat, and momentum play an important role in the climate system of the tropics. This study examines air-sea fluxes and assesses the theoretical understanding of these fluxes by comparing aircraft data to the ERA5 reanalysis model. During the 2011 DOMEX project, aircraft measurements of atmospheric conditions were gathered over twenty flights at 300m and 1200m above sea level, near Dominica, in the western tropical Atlantic. In this study, the eddy correlation method is used to calculate the mean conditions of fluxes and investigate their vertical profiles through the sub-cloud layer. The aircraft measurements yield flux values fairly consistent with vertical profiles generated by large eddy simulation models (Siebesma et al., 2003).

The ERA5 reanalysis model is compared to the aircraft data to assess model parameterizations of air-sea interface fluxes. Despite very close correlations in wind speed values, the ERA5 model produces systematically greater values for temperature and humidity difference at the surface (ΔT and Δq), and does not fully reflect the day-to-day variations measured by the aircraft. The empirical transfer coefficient for latent heat bulk transfer ($C_Q = 1.2\text{x}10^{-3}$) is greater than the model's coefficient values, and the coefficient for sensible heat flux bulk transfer ($C_H = 1.0\text{x}10^{-3}$) is less than the model's values. The ERA5 parameterizations for the drag coefficient result in momentum fluxes with higher sensitivities to wind speed. These findings suggest that, while the ERA5 parameterizations better reflect variations in boundary layer transfer schemes than empirical transfer coefficients, the model exhibits bias in high sensible heat fluxes and does not fully capture day-to-day atmospheric variation measured by the aircraft.

Contents

1. Introduction

1.1. Air-Sea Fluxes and Tropical Climate

Air-sea flux is an important mechanism in atmospheric boundary layer dynamics. In particular, vertical fluxes at the ocean-atmosphere interface are key vertical transport phenomena in the sub-cloud layer and affect the surface energy budget. Understanding the surface energy budget and the turbulent dynamics in the boundary layer is imperative to complete understanding of climate dynamics (LeMone et al., 2019; Haiden, 1996). Vertical fluxes in the boundary layer play a role both in short timescale dynamics like cloud formation, and in long timescale climate phenomena like El Niño (Kumar et al., 2011). In the tropics, these fluxes affect shallow cumulus convection and vertical transport throughout the cumulus layer. Trade wind cumulus convection is a major source of heat in the atmosphere and of moisture under the subsiding branch of the Hadley cell. Therefore, air-sea fluxes in the tropical oceans play a key role in general atmospheric circulation (Siebesma and Cuijpers, 1994; Siebesma et al., 2003).

1.2. Previous Air-Sea Flux Studies

Previous studies of air-sea fluxes in the tropics have used a variety of measurements from instruments on moored buoys, ships, and aircrafts. BOMEX was an early project designed to study air-sea fluxes and surface energy budgets in the western tropical Atlantic using ship and aircraft measurements. The results of the BOMEX project led to a greater understanding of boundary layer eddy size and shear, and confirmed aircraft measurement agreement with other methods of estimating fluxes (Kuettner and Holland, 1969; Paulson et al., 1972; Holland, 1972). GATE was another large project involving over 70 countries, and a system of measurements by buoys, ships and aircrafts. The boundary layer subprogram of GATE made measurements of fluxes, estimated bulk transfer coefficients and produced vertical profiles of fluxes (Kuettner, 1974; Hoeber, 1974; Thompson et al., 1980). ATEX was a third study of air-sea fluxes under the trade winds using eddy correlation method to measure fluxes from ships and buoys. In addition, ATEX used radiosondes to measure the thermodynamic profile of the atmosphere in the trade winds, to better investigate the vertical variation of fluxes (Dunkel et al., 1974; Augstein et al., 1974).

2. Data and Model

2.1. The Dominica Experiment

The Dominica Experiment (DOMEX) was a field campaign in April and May of 2011, with primary goal of studying orographic precipitation on the island of Dominica, in the western tropical Atlantic Ocean. DOMEX used the University of Wyoming King Air Research Aircraft to collect data on 21 flights, each including flight legs through the undisturbed trade winds upstream of Dominica. Figure 2.1.1. shows the flight paths of the aircraft. This study uses measurements take on Leg 1, the upstream leg, at both 300m and 1200m above sea surface. The King Air research aircraft measured wind speed and thermodynamic properties of the atmosphere, creating a dataset well-suited for analyzing tropical atmospheric convection and vertical fluxes of latent heat, sensible heat, and momentum (Smith et al., 2012).

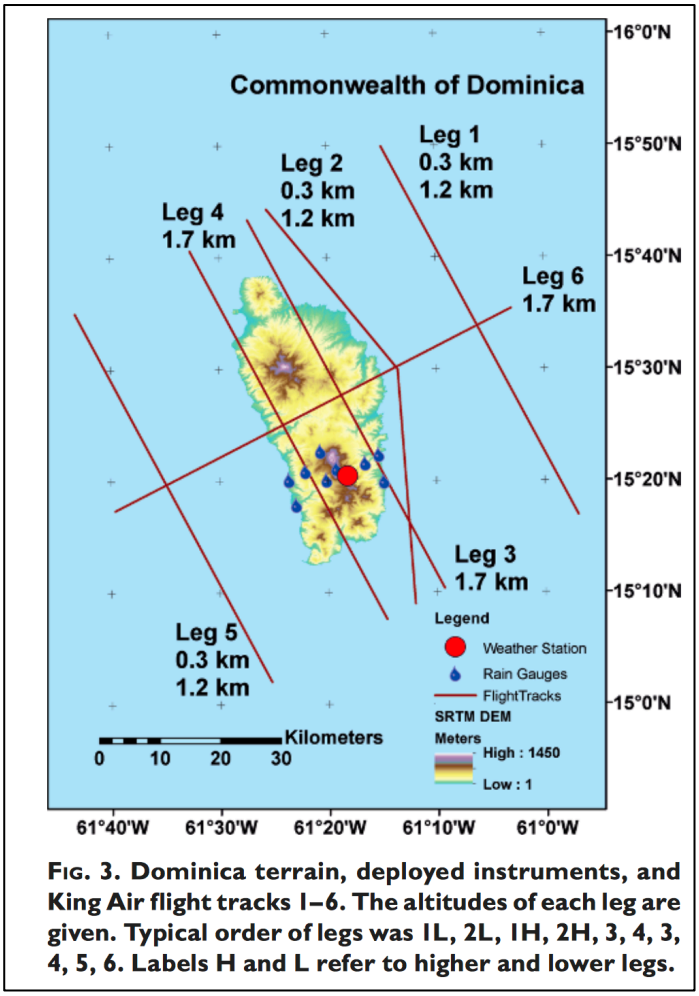

FIG. 3. Dominica terrain, deployed instruments, and King Air flight tracks 1–6. The altitudes of each leg are given. Typical order of legs was 1L, 2L, 1H, 2H, 3, 4, 3, 4, 5, 6. Labels H and L refer to higher and lower legs.

Figure 2.1.1. Map of DOMEX flight paths (After Smith et al., 2012).

2.2. ERA5 Reanalysis Model

ERA5 is the newest iteration of the European Center for Midrange Weather Forecasts (ECWMF) reanalysis model of global weather and climate. It includes reanalysis data from 1979 to present on hourly time steps, with 31km horizontal resolution. The ERA5 model compares well with other reanalysis products, such as MERRA-2 and JRA-55 (Hersbach et al., 2019). Furthermore, Kumar, et al. (2012) find that ERA-Interim, the predecessor to ERA5, performed better than both NCAR reanalysis products, NCEP-1 and NCEP-2, in calculating air-sea fluxes.

3. Methods

3.1. Flux Method 1. Aircraft Flight-Level Fluxes calculated with eddy correlation method

Nineteen DOMEX flights measured data on the 70km-long legs, upwind of the island of Dominica at two flight levels. The appendix includes a list of data from the DOMEX dataset used in this project, as well as the instruments on the aircraft used to measure them. To understand the vertical profile of fluxes of sensible heat, latent heat, and momentum over the ocean, this study calculates fluxes from in situ aircraft measurements flight legs at two heights (300m and 1200m), using the eddy correlation method.

Eddy correlation method calculates the perturbation values of wind speed, moisture and temperature to produce a time series which is then averaged over a time or space integral. Mathematically, eddy correlation method infers the source or sink strength of a scalar quantity by measuring perturbations of the atmospheric quantity. It is a direct method of calculating fluxes at the height and location of the time series, in this case, along the flight path at 300m and 1200m (Lee, 2018). The vertical turbulent flux of a variable, A, is defined by a product of perturbations, $\overline{w'A'}$, where w is the vertical component of wind speed (Stull, 1998).

The average vertical flux over a flight leg for a variable, A, can be calculated through a space integral:

$$\text{Flux} = \rho\, C\, \frac{1}{l} \int_{start}^{end} w'A'dx \qquad (1)$$

where

$$w' = w(x) - \bar{w}\ ;\ A' = A(x) - \bar{A} \qquad (2)$$

and C is a constant pertinent to A (i.e. heat capacity for sensible heat flux, or latent heat of evaporation for latent heat flux). The same vertical flux can also be calculated through a time integral:

$$\text{Flux} = \rho\, C \frac{1}{T} \int_{start}^{end} w'A'dt \quad (3)$$

In either case, the average vertical flux for a flight leg can be calculated by averaging the perturbation of the vertical wind and of the variable pertinent to the flux:

$$\text{Average Flux} = \rho\, C\, \overline{w'A'} \quad (4)$$

Each calculation includes the density of air, which is calculated with the ideal gas law from pressure and temperature values from aircraft measurements, with the specific gas constant of air, $R_{air} = 287 J\ kg^{-1}\ K^{-1}$.

$$\rho = \frac{P}{R_{air}T} \quad (5)$$

The pertinent atmospheric quantity for sensible heat flux is the dry potential temperature (θ), a calculated variable in the King Air dataset. This flux also includes the heat capacity of air, $c_p = 1004 J\ kg^{-1}\ K^{-1}$. Therefore, the flight averages of sensible heat flux are calculated, in units of Wm^{-2}:

$$\text{SHF} = \rho\, c_p\, \overline{w'\theta'} \quad (5)$$

Similarly, the pertinent atmospheric quantity for latent heat flux is the specific humidity (q), calculated from the aircraft measurement of the water vapor mixing ratio, where

$$q = \frac{mr}{1+mr} \quad (6)$$

This flux also includes the latent heat of evaporation, a constant $L = 2.5 \times 10^6\ J\ kg^{-1}$.

Therefore, the flight averages of latent heat flux are calculated, in units of Wm^{-2}:

$$\text{LHF} = \rho\, L\, \overline{w'q'} \quad (7)$$

The momentum flux is calculated with the perturbations of the zonal and meridional wind components (separately), in units of $N\ m^{-2}$ (Pa):

$$\text{UMF} = \rho\, \overline{w'u'} \quad (8)$$

$$\text{VMF} = \rho\, \overline{w'v'} \quad (9)$$

3.2. Flux Method 2. Surface fluxes calculated with bulk laws and aircraft data

The bulk laws are based on the theoretical understanding that vertical fluxes at the ocean-atmosphere interface are driven by temperature and humidity differences between the atmosphere and a thin layer of air in equilibrium with the surface of the ocean (Stull 1998, Stewart 2008). Each bulk law has the general form of

$$\text{Surface Flux} = \rho\, C\, U\, \Delta A \tag{10}$$

where air density is calculated from the ideal gas law (Eqn. 5), U is the magnitude of wind speed, A is a given quantity and C is the corresponding bulk transfer coefficient. U is calculated from the measured wind speed components (Eqn. 11), and extrapolated to the surface with the power law (Eqn. 12 & 13).

$$U = \sqrt{u^2 + v^2} \tag{11}$$

$$\frac{U_{Z1}}{U_{Z2}} = \left(\frac{Z_1}{Z_2}\right)^{\frac{1}{7}} \tag{12}$$

$$U_{10m} = \frac{(U_{FL})}{\left(\frac{FL}{10m}\right)^{\frac{1}{7}}} \tag{13}$$

Sensible Heat Flux

For sensible heat flux, the air temperature of the thin layer at the ocean-atmosphere interface is assumed to be equal to the sea surface temperature, which is measured by an IR device on the aircraft. The temperature of the atmosphere just above the surface is calculated by extrapolating the temperature from the lower flight leg to the surface using the dry adiabatic lapse rate (Γ=-gz). Therefore,

$$\Delta T = SST - T_{air} \tag{14}$$

$$T_{air} = T_{FlightLevel} - gz \tag{15}$$

The bulk law for sensible heat flux is

$$SHF = \rho\, c_p\, C_H\, U\, \Delta T \tag{16}$$

c_p is the specific heat of air (c_p=1004J kg^{-1} K^{-1}), and the unitless constant, C_H, is the sensible heat transfer coefficient and is empirically determined. The value cited by Stewart (2008), of $C_H = 1x10^{-3}$ is used.

Latent Heat Flux

For latent heat flux, the specific humidity of the thin layer of air at the ocean interface is assumed to be in equilibrium with the ocean. It is, therefore the specific humidity at

saturation determined by the air temperature of the layer (SST). Section 8 includes the full calculation of the specific humidity at saturation using a polynomial approximation for the Clausius-Clapeyron Relation (Lowe, 1976). Assuming that specific humidity is conserved, the specific humidity of the atmosphere at the surface is equal to the specific heat at flight level. Therefore,

$$\Delta q = q_{sat} - q_{flightlevel} \quad (17)$$

The bulk law for latent heat flux is

$$LHF = \rho\, L\, C_Q\, U\, \Delta q \quad (18)$$

L is the latent heat of evaporation ($L=2.5x10^6 J\ kg^{-1}$), and the constant, C_Q, is the latent heat transfer coefficient and is empirically determined, $C_Q = 1.2x10^{-3}$ (Stewart, 2008).

Momentum Flux

Momentum flux at the surface is driven by the square of the wind speed near the surface. Wind speed at ten meters is calculated by the power law (Eqn. 13). The bulk law for zonal and meridional momentum flux is

$$UMF = \rho\, C_D\, u^2 \quad (19)$$

$$VMF = \rho\, C_D\, v^2 \quad (20)$$

The constant, C_D, is the drag coefficient, with an empirical value of $C_D = 1x10^{-3}$ (Sahlée et al., 2008).

Empirical values for the transfer coefficients lead to variations in results of surface fluxes. Stull (1988) suggests that, in statically neutral conditions, $C_H=C_Q$ and values range 1-$5x10^{-3}$. Stewart (2008) gives specific values of $C_H = 1.0x10^{-3}$ and $C_Q = 1.2x10^{-3}$. More so than the transfer coefficients for latent heat and sensible heat, the drag coefficient for wind (C_D) varies by study and wind scheme. Smith (1988) finds that the wind coefficient increases from $1x10^{-3}$ at winds around 5ms/, to $2x10^{-3}$ at 24m/s. Other sources (Gill, 1982 and Stewart, 2008) cite schemes for drag coefficients with linear dependencies on wind speed. The surface winds in this study are generally under 5m/s, so the value of $C_D = 1x10^{-3}$ is used (Sahlée et al., 2008).

3.3. Flux Method 3. ERA5 parameterizations for surface fluxes

To compare the ERA5 parameterizations for surface fluxes to the aircraft measurements fluxes, the data are time-averaged for the window of 14:00-20:00 UTC

(10:00-16:00 AST). This is the daily flight window of the DOMEX study. The data is spatially averaged from a 9x9 matrix of points over the area of 60-62ºW by 14-16ºN. To calculate surface fluxes, the ERA5 model uses the same bulk law:

$$SHF = \rho\, c_p\, C_H\, U\, \Delta T \quad (14)$$

$$LHF = \rho\, L\, C_Q\, U\, \Delta q \quad (16)$$

$$MF = \rho\, C_M\, U^2 \quad (19)$$

The ECMWF uses the convention of downward positive flux, so the sign of the ERA5 flux values are flipped to compare the model to the aircraft data. The ERA5 parameterizations differ from Method 2 in definitions for the bulk transfer coefficients. While Method 2 uses empirically determined constants for transfer coefficients, the model uses Monin-Obukhov similarity theory to write these coefficients in terms of profile functions and stability functions (functions of the Monin-Obukhov length, L, and surface roughness length, z_0). The coefficients are defined, after IFS Documentation:

$$C_M = \frac{\kappa^2}{\left[\log\left(\frac{z_n+z_{0M}}{z_{0M}}\right) - \Psi_M\left(\frac{z_n+z_{0M}}{\mathcal{L}}\right) + \Psi_M\left(\frac{z_{0M}}{\mathcal{L}}\right)\right]^2}$$

$$C_H = \frac{\kappa^2}{\left[\log\left(\frac{z_n+z_{0M}}{z_{0M}}\right) - \Psi_M\left(\frac{z_n+z_{0M}}{\mathcal{L}}\right) + \Psi_M\left(\frac{z_{0M}}{\mathcal{L}}\right)\right]\left[\log\left(\frac{z_n+z_{0M}}{z_{0H}}\right) - \Psi_H\left(\frac{z_n+z_{0M}}{\mathcal{L}}\right) + \Psi_H\left(\frac{z_{0H}}{\mathcal{L}}\right)\right]}$$

$$C_Q = \frac{\kappa^2}{\left[\log\left(\frac{z_n+z_{0M}}{z_{0M}}\right) - \Psi_M\left(\frac{z_n+z_{0M}}{\mathcal{L}}\right) + \Psi_M\left(\frac{z_{0M}}{\mathcal{L}}\right)\right]\left[\log\left(\frac{z_n+z_{0M}}{z_{0Q}}\right) - \Psi_Q\left(\frac{z_n+z_{0M}}{\mathcal{L}}\right) + \Psi_Q\left(\frac{z_{0Q}}{\mathcal{L}}\right)\right]}$$

The roughness lengths for the surface are given by

$$z_{0M} = \alpha_M \frac{\nu}{u_*} + \alpha_{Ch} \frac{u_*^2}{g}$$

$$z_{0H} = \alpha_H \frac{\nu}{u_*}$$

$$z_{0Q} = \alpha_Q \frac{\nu}{u_*}$$

where g is the gravitational constant, u_* is the friction velocity (a scaling parameter), ν is the kinematic viscosity ($\nu = 1.5\text{x}10^{-5}$ m^2s^{-1}), $\alpha_M = 0.11$, and the Charnock coefficient is $\alpha_{Ch} = 0.018$. The Von Karman constant, κ, is approximately equal to 0.4 in these calculations (Beljaars, 1997), and z_n is the height of the first model layer (10m, the reference height for wind speed).

The physical interpretation of the Monin-Obukhov length, L, is the height at which buoyant destruction of turbulence is equal to the shear production of turbulent energy.

When z>>L, effects of stratification dominate, and turbulence is forced by buoyancy, whereas when z<<L, wind shear dominates and forces turbulence (Kundu and Cohen, 1990). ERA5 parameters define $\zeta = z/L$ so that stable conditions are $\zeta > 0$. For stable conditions, the stability functions, as empirical functions, are (after IFS Documentation):

$$\Psi_M(\zeta) = -b\left(\zeta - \frac{c}{d}\right)\exp(-d\zeta) - a\zeta - \frac{bc}{d}$$

$$\Psi_H(\zeta) = \Psi_Q(\zeta) = -b\left(\zeta - \frac{c}{d}\right)\exp(-d\zeta) - \left(1 + \frac{2}{3}a\zeta\right)^{1.5} - \frac{bc}{d} + 1$$

where $a = 1$, $b = 2/3$, $c = 5$, and $d = 0.35$.

As Lee (2018) notes in defining similar transfer coefficients for bulk laws, the Monin-Obukov scheme with profile functions requires iterative calculations and an initial guess for the wind profile to determine *Ψ, L, and* z_{0m}.

3.4. Flux Method 4. Surface fluxes calculated with bulk laws and ERA5 conditions

Method 4 uses the same bulk law calculations as Method 2, but uses atmospheric quantities from the ERA5 model. Once again, each bulk law has the general form of

$$\text{Surface Flux} = \rho\, C\, U\, \Delta A \qquad (25)$$

where air density is calculated from the ideal gas law (Eqn. 5), U is calculated by the power law (Eqn. 11).

Sensible Heat Flux

For sensible heat flux, the temperature of the thin layer at the ocean-atmosphere interface is assumed equal to the sea surface temperature, given in the ERA5 dataset. ERA5 produces variable of temperature at 2m above the surface to be the other air temperature driving the flux. So,

$$\Delta T = SST - T_{2m} \qquad (26)$$

$$SHF = \rho\, c_p\, C_H\, U\, \Delta T \qquad (27)$$

The constant, C_H, is the sensible heat transfer coefficient and is empirically determined, with the same value of $C_H = 1x10^{-3}$ (Stewart, 2008).

Latent Heat Flux

For latent heat flux, the specific humidity of the thin layer of air at the ocean interface is in assumed to be in equilibrium with the ocean and is the specific humidity at saturation.

The polynomial approximation for the Clausius-Clapeyron Relation is used to calculate the specific humidity at saturation from SST (Lowe, 1976). ERA5 produces specific humidity of the atmosphere near the surface (at 1000hPa). Therefore,

$$\Delta q = q_{sat} - q_{1000hPa} \quad (28)$$

$$LHF = \rho\, L\, C_Q\, U\, \Delta q \quad (29)$$

The constant, C_Q, is the latent heat transfer coefficient and is empirically determined, with a value of $C_Q = 1.2x10^{-3}$ (Stewart, 2008).

Momentum Flux

Momentum flux at the surface is driven by the square of the wind speed 10m above the surface. The bulk laws for zonal and meridional momentum flux, respectively, are

$$UMF = \rho\, C_D\, u^2 \quad (30)$$

$$VMF = \rho\, C_D\, v^2 \quad (31)$$

The drag coefficient has an empirical value of $C_D = 1x10^{-3}$ (Sahlée et al., 2008).

3.5. Uncertainties and Error

The eddy correlation method has uncertainties in measurements and in the calculations, which use measured moments in place of idealized ensemble-averaged moments (Lenschow et al., 1993). The 1993 study, "How Long is Long Enough When Measuring Fluxes and Other Turbulence Statistics," determines an upper bound for the systematic error in eddy covariance calculations of fluxes. The error estimates are determined by variances of the vertical wind velocity and the other variables (humidity, temperature, wind speed) and on the integral time scale of the vertical velocity. This yields uncertainties in the eddy correlation method of 33% for zonal momentum flux, 69% for meridional momentum flux, 20% for latent heat flux, and 27% for sensible heat flux. Lenschow's study also determines the necessary flight length for an aircraft measuring fourth-order moments with an error less than 10% to be 90km. The DOMEX flights are short of this by approximately 20km.

In comparison, a similar study of fluxes over land using eddy correlation method and the UW King Air research aircraft found that average uncertainties for vertical fluxes was 40% for latent heat flux and 30% for sensible heat flux (Betts et al., 1990). Based on average

flux values for Method 1, this is ± 38 W/m^2 for latent heat flux and ± 1.7W/m^2 for sensible heat flux.

For the bulk laws, the greatest discrepancies result from the variation of coefficient definitions. Knauss and Garfield (2017) state that typical variations in different coefficients (C_Q and C_H) can lead to 30% variation in latent heat and sensible heat fluxes. In considering the coefficient for and momentum flux (C_D or C_M), Stewart (2008) states that drag coefficient error can lead to a 10% variation in wind stress. Deardorff (1968) makes a qualitative assessment of the error caused by estimated coefficients in stable conditions: all air-sea differences are increased with stable stratification, so the coefficients are too large when estimated from neutral values in stable stratification.

4. Results/Discussion on Aircraft Fluxes

4.1. Overview of Results (Mean and Daily Variation of Fluxes)

Table 4.1.1 shows the results of flux calculations from the aircraft data. The latent heat fluxes are orders of magnitude larger than the sensible heat fluxes at the surface and at the low flight level. Momentum fluxes, driven by the easterly trade winds, are very small, and smaller in the meridional direction than the zonal direction.

Latent heat fluxes show the greatest daily variation in the high flight leg, and exhibit the least amount of daily variation at the surface. There are instances of negative (downward) latent heat fluxes at the flight levels, but not at the surface. Furthermore, the low flight leg latent heat flux is always less positive than the surface latent heat flux. From this, one can infer a convergence of latent heat flux between the surface and the low flight leg.

For sensible heat flux, the high flights show the greatest range, from nearly -50Wm^{-2} to +70Wm^{-2}. However, the values of sensible heat flux for the low flight level and the surface hover around 0 Wm^{-2}, and all three vertical levels include instances of both positive (upward) and negative (downward) sensible heat flux. The values are small enough that fluctuations around zero may be attributed to measurement uncertainty. It is characteristic of the tropics to have very small surface sensible heat fluxes because of the warm sea surface temperatures and warm air temperatures.

All of the surface level fluxes of zonal momentum are positive, but small, values. As is the case with the other fluxes considered, the high flight leg has the greatest variability in values, both positive and negative. In comparison to the zonal momentum fluxes, the meridional momentum flux values are quite small. The direction of momentum flux is determined by wind direction, easterly trade winds and small northerly components result in positive flux values.

	LHF	(W/m^2)		SHF	(W/m^2)	
Flight	Low	High	Surface	Low	High	Surface
1	145.328	88.354	230.861	-0.577	-16.722	-3.8772
3	147.037	50.773	190.989	-1.628	-4.533	0.4
4	88.363	490.456	126.611	-0.287	-26.593	-0.2023
5	57.038	761.864	67.3132	5.498	49.403	-0.8959
6	42.984	-32.914	72.3289	0.542	-2.812	-1.5848
7	90.919	-31.533	80.7629	-1.447	6.644	2.4234
8	62.988	-66.302	64.911	2.955	2.396	1.0737
9	63.735	-1.335	82.3002	1.684	24.843	1.9993
10	3.849	-11.770	126.792	0.008	1.163	1.8322
11	79.979	26.880	170.802	3.640	-9.265	0.4002
12	42.390	-51.378	213.922	2.444	10.267	-4.0888
13	145.355	25.657	234.946	-1.702	-9.480	0.1293
14	58.546	13.947	154.227	3.682	-0.717	-3.669
15	19.848	321.545	182.908	-18.402	33.172	2.5338
16	147.289	22.821	174.163	-6.647	7.335	-3.3301
17	56.916	-25.532	135.368	0.088	4.304	-4.6831
18	88.223	273.511	93.0961	-2.077	72.660	0.378
19	63.786	188.031	84.7235	-20.241	-49.178	-1.0405
Mean	78.032	113.504	138.168	-1.804	5.160	-0.678
Max.	147.289	761.864	234.946	5.498	72.660	2.534
Min.	3.849	-66.302	64.911	-20.241	-49.178	-4.683

	UMF	(N/m^2)		VMF	(N/m^2)	
Flight	Low	High	Surface	Low	High	Surface
1	0.086	-0.045	0.065	-0.004	-0.015	0.001
3	0.025	0.002	0.039	0.003	0.002	0.002
4	0.025	0.061	0.025	0.001	-0.231	0.000
5	0.024	-0.042	0.014	0.022	-0.180	0.000
6	0.018	-0.037	0.013	-0.018	-0.030	0.001
7	0.019	0.007	0.001	0.007	0.015	0.007
8	0.020	-0.016	0.004	-0.007	-0.025	0.001
9	0.028	0.049	0.004	-0.041	0.011	0.003
10	0.005	-0.003	0.022	-0.018	-0.001	0.000
11	0.007	-0.030	0.042	-0.023	0.001	0.000
12	0.089	-0.012	0.069	0.006	0.029	0.000
13	0.137	-0.009	0.094	-0.010	0.056	0.002
14	0.037	-0.011	0.040	-0.013	0.029	0.000
15	-0.008	-0.114	0.063	0.040	-0.062	0.001
16	0.051	-0.107	0.056	-0.007	-0.076	0.002
17	0.031	0.004	0.036	-0.010	0.019	0.001
18	0.129	-0.188	0.019	-0.070	0.095	0.000
19	-0.044	-0.177	0.045	-0.061	-0.232	0.001
Mean	0.038	-0.037	0.036	-0.011	-0.033	0.001
Max.	0.137	0.061	0.094	0.040	0.095	0.007
Min.	-0.044	-0.188	0.001	-0.070	-0.232	0.000

Table 4.1.1. Summary of Aircraft Flux Calculations. "Low" (300m) and "High" (1200m) are flight level fluxes calculated by Method 1, and "Surface" fluxes are calculated by Method 2.

4.2. Vertical Variation in Fluxes

A theoretical understanding of how these vertical fluxes vary with elevation is proposed through a large eddy simulation study in 2003 by Siebesma, et al., in "A Large Eddy Simulation Intercomparison Study of Shallow Cumulus Convection." This study, of fluxes in tropical cumulus convection, is a point of comparison to the fluxes calculated from the aircraft data. Figure 4.2.1 shows vertical profiles of fluxes as produced by large eddy simulation (LES) models from the 2003 paper. Average values of each flux as calculated from aircraft data, have been marked on the graphs at the appropriate heights. The greatest range of flux values from aircraft data occurs at the 1200m flight level and coincides with increased uncertainties in the LES models.

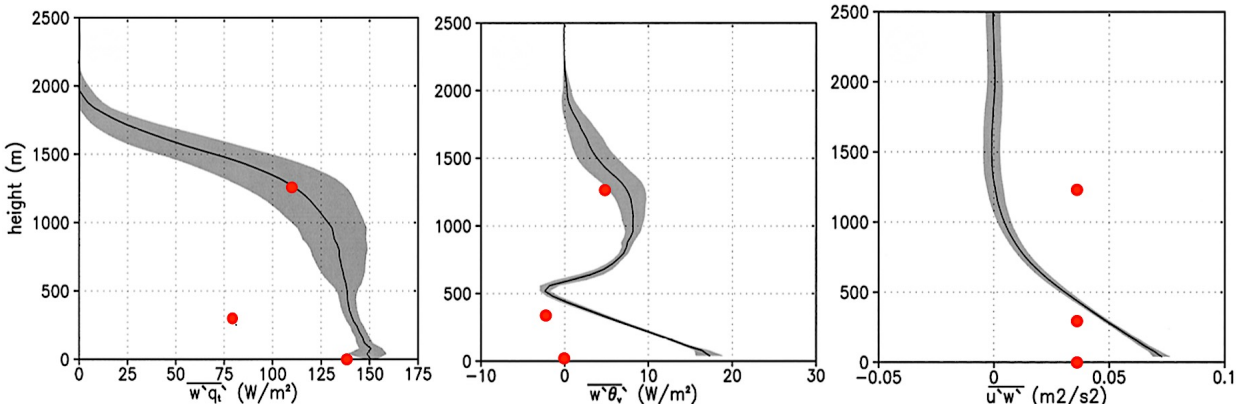

(a) (b) (c)

Figure 4.2.1. After Siebesma, et al. (2003). Vertical profiles of total water flux (a), virtual potential temperature flux (b), and momentum flux (c). Grey profiles are from Siebesma, et al. (2003), and red marks indicate average flux values from DOMEX aircraft data.

The vertical profiles of fluxes suggest divergence and convergence of fluxes. If there is a strong upward flux at the surface, but a weaker or a downward flux at higher levels, there must be another mechanism for transport besides vertical flux. To reconcile convergence and divergence, schematic diagrams of other mechanisms of transport are presented in Figure 4.2.2. Besides vertical turbulent fluxes, advection is a horizontal means of transport for all three quantities. Radiation may have an effect on sensible heat flux values and their vertical convergence between levels, and friction could affect the momentum flux values and account for vertical convergence. The LES model's vertical profiles in Figure 4.2.1, and the schematics of heat and momentum transfer in Figure 4.2.2 offer a theoretical foundation for analyzing the fluxes calculated from aircraft data.

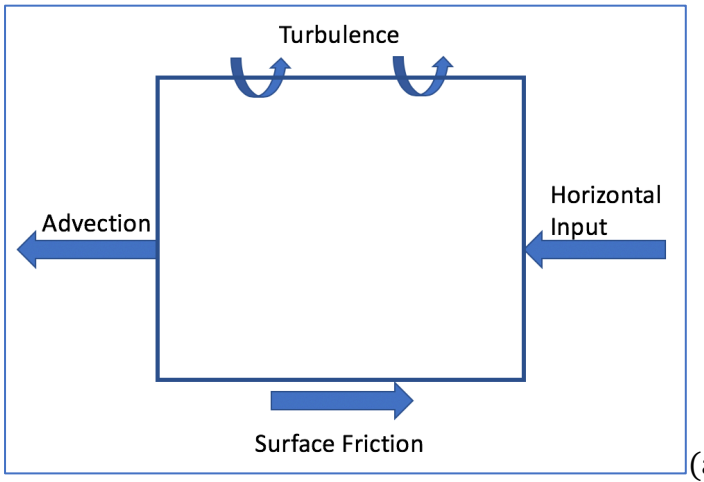

(a)

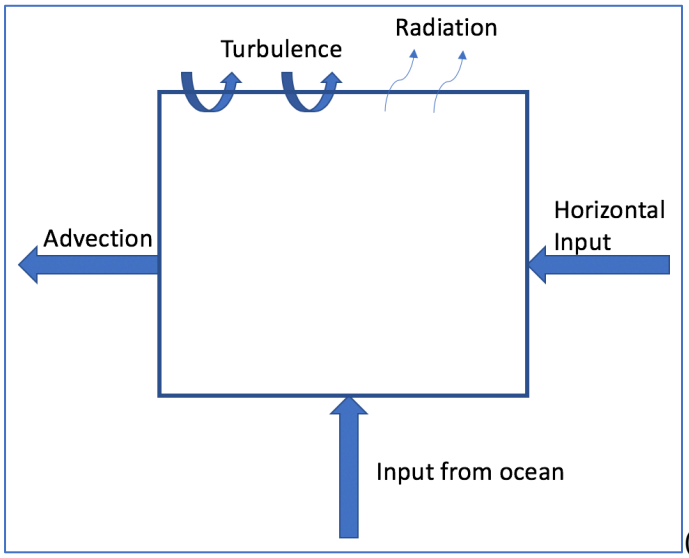

(b)

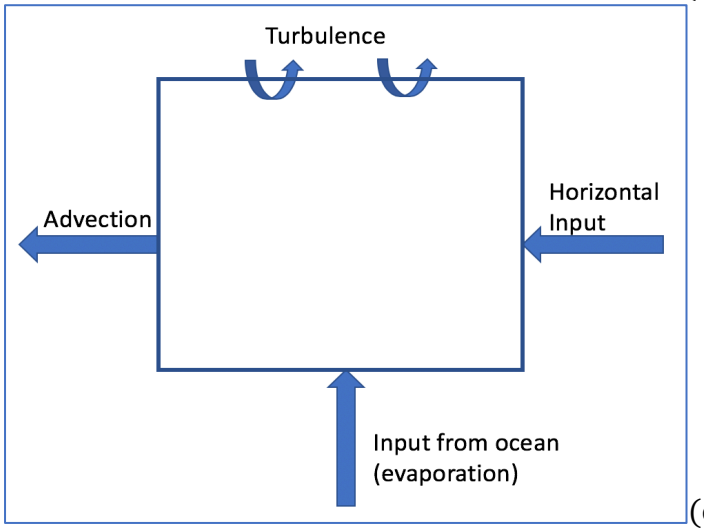

(c)

Figure 4.2.2. Schematic Diagrams of transport mechanisms for Momentum (a), Sensible Heat (b), and Latent Heat (c) in an air parcel.

4.2(a) Flight Level Fluxes: Vertical Variation

Comparison of fluxes at the different flight levels assesses vertical variation in fluxes, and the relationship between fluxes at different levels. The high flight leg was flown around 1200m, and the low flight leg was flow around 300m. Using a simple calculation with relative humidity (after Lawrence, 2005), the lifted condensation level (LCL) is estimated around 500m on average, so the aircraft was flying below the LCL in the low flight leg and above it in the high flight leg. Figure 4.2.3 compares the fluxes from the low leg and the high leg. There is little correlation between fluxes at the two levels, suggesting that the vertical variation of fluxes is non-linear between the two levels. The LCL and the presence of the cloud layer in the high flight level offers a partial explanation for the lack of correlation between fluxes at 300m and 1200m.

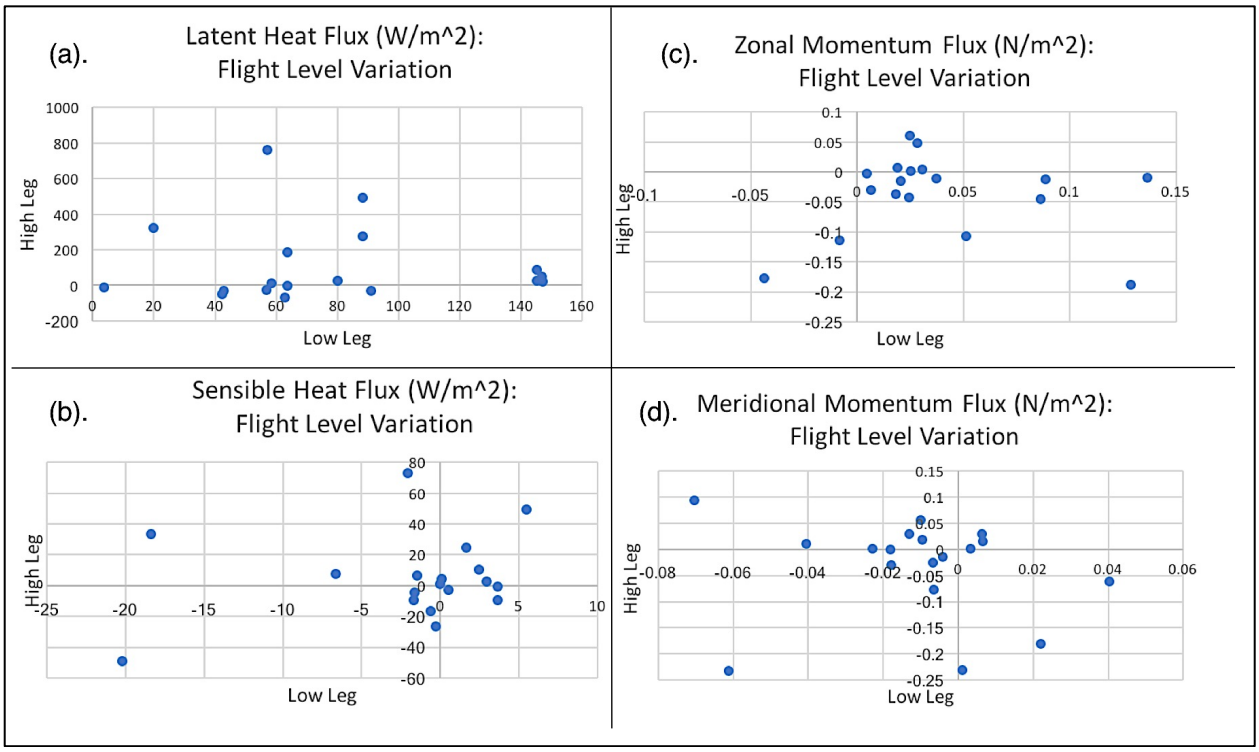

Figure 4.2.3. Flux comparison for Low Flight Legs and High Flight Legs. All Fluxes are calculated with Method 1 (eddy correlation method). Latent Heat Flux shown in (a), Sensible Heat Flux in (b), Zonal Momentum Flux (c), and Meridional Momentum Flux (d).

4.2(b) Surface Fluxes and Flight Level Fluxes (below LCL): Vertical Variation

Comparison of surface fluxes and flight level fluxes is not direct, and depends on both vertical variation and differences between eddy correlation method and the bulk law. Figure

4.2.4 compares the latent heat flux at the surface and at the low flight leg (around 300m). There is small correlation between the two methods (R^2=0.20265), shown in comparison to a one-to-one correlation in the figure.

The values at the surface trend higher than the values at the low flight level, indicating a convergence of fluxes. In reference to Figure 4.2.2(c), this may be resolved with latent heat transport by advection. Siebesma, et al. (2003) suggests that latent heat flux decreases marginally throughout the sub-cloud layer, up to about 1500m, at which height it decreases strongly because of the capping of the trade wind inversion. The strong decrease expected by LES models is inconsistent with the aircraft latent heat flux in the high leg.

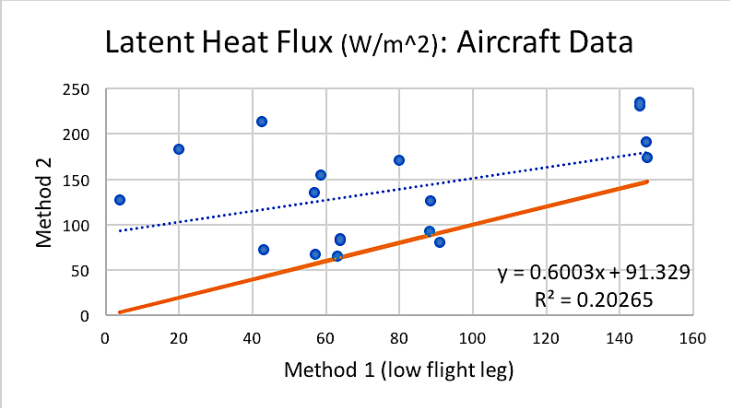

Figure 4.2.4. Latent Heat Fluxes at the surface (Method 2) and at the low flight level (Method 1). The blue dotted line shows the linear regression, and the orange line marks a one-to-one correlation line. Note the higher values at the surface.

Figure 4.2.5 shows the sensible heat fluxes at the surface and at the low flight level. While Siebesma, et al. (2003) suggests that sensible heat flux should decrease linearly with height to the cloud base, there is no such trend in the aircraft data (linear trend R^2=0.03181). Both methods yield negative values for sensible heat flux, which the LES model predicts around 500m. The model also puts forth a vertical profile for zonal momentum flux decreasing to zero at the cloud layer. Figure 4.2.6 shows the zonal momentum flux results from the aircraft. The linear trend does indicate that the fluxes at flight level are generally smaller than the fluxes at the surface, as suggested by the LES model's vertical profiles. Meridional momentum flux (Figure 4.2.7) is small, and not discussed by the LES study.

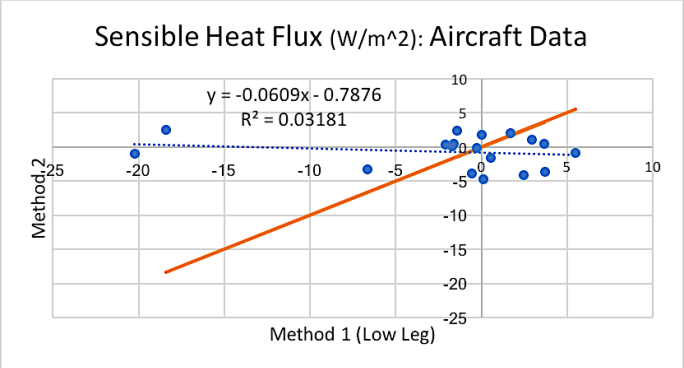

Figure 4.2.5. Sensible Heat Fluxes at the surface (Method 2) and at the low flight level (Method 1).

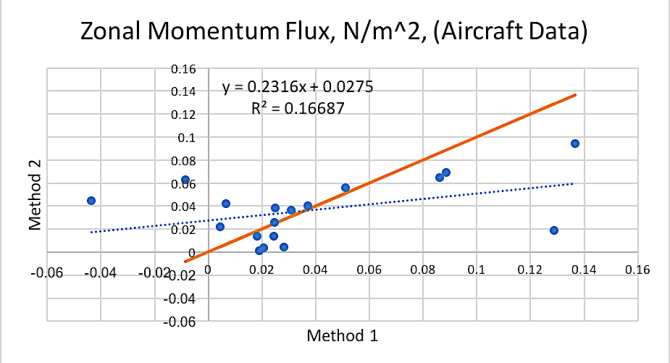

Figure 4.2.6. Zonal Momentum Fluxes at the surface (Method 2) and at the low flight level (Method 1).

4.3. Sensitivities in Fluxes: Comparison of Method 1 and Method 2

To investigate the daily variation in flux values, the various atmospheric conditions that might affect vertical fluxes of heat, moisture, and momentum are considered. One indication of the atmospheric conditions that affect these fluxes is in the bulk law used to calculate the flux at the surface. Therefore, Method 1 (eddy correlation method) and Method 2 (bulk laws), are compared in sensitivities to atmospheric quantities that make up the bulk laws.

Momentum flux at the surface, as determined by the bulk laws (Method 2), goes as the square of the wind speed. Figure 4.3.1. shows the zonal momentum flux (UMF) as a function of wind speed. The surface level fluxes (orange) are directly calculated from U^2, and follow the square of the wind speed (Eqn. 19). A parabolic curve through the origin does not fit to UMF at flight level very well (R^2=0.14). However, the parabolic curve fit is very close to the curve fit for the surface level fluxes.

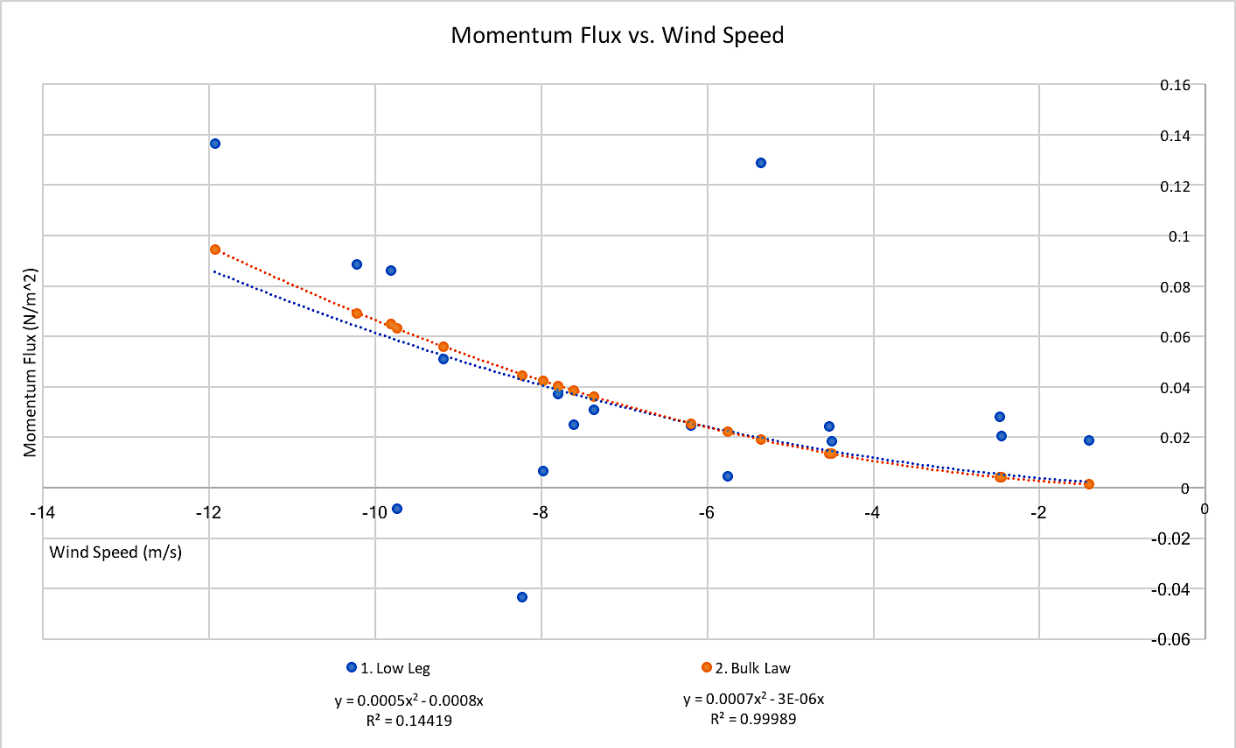

Figure 4.3.1. Wind Speed and Momentum Flux as calculated by Method 1 (Low Leg) and Method 2 (Bulk Law). Curve fits are parabolas through the origin. Wind speed values are negative because the trade winds are easterly winds.

Figures 4.3.2 and 4.3.3 similarly examine the atmospheric variables that constitute the bulk laws for correlation sensible heat flux and latent heat flux, respectively. Based on Equation 16 and Equation 18, latent heat flux depends on the product of wind speed (u) and the difference in relative humidity (Δq), and sensible heat flux depends on both wind speed (u) and the temperature difference (ΔT). Unlike the momentum fluxes, there is no correlation between the linear fit of the products from the bulk law ($u*\Delta q$ and $u*\Delta T$) and latent heat flux or sensible heat flux. The results from the sub-cloud layer do not reflect the sensitivities of the bulk laws, so the surface conditions cannot be extrapolated from the surface to predict vertical fluxes aloft.

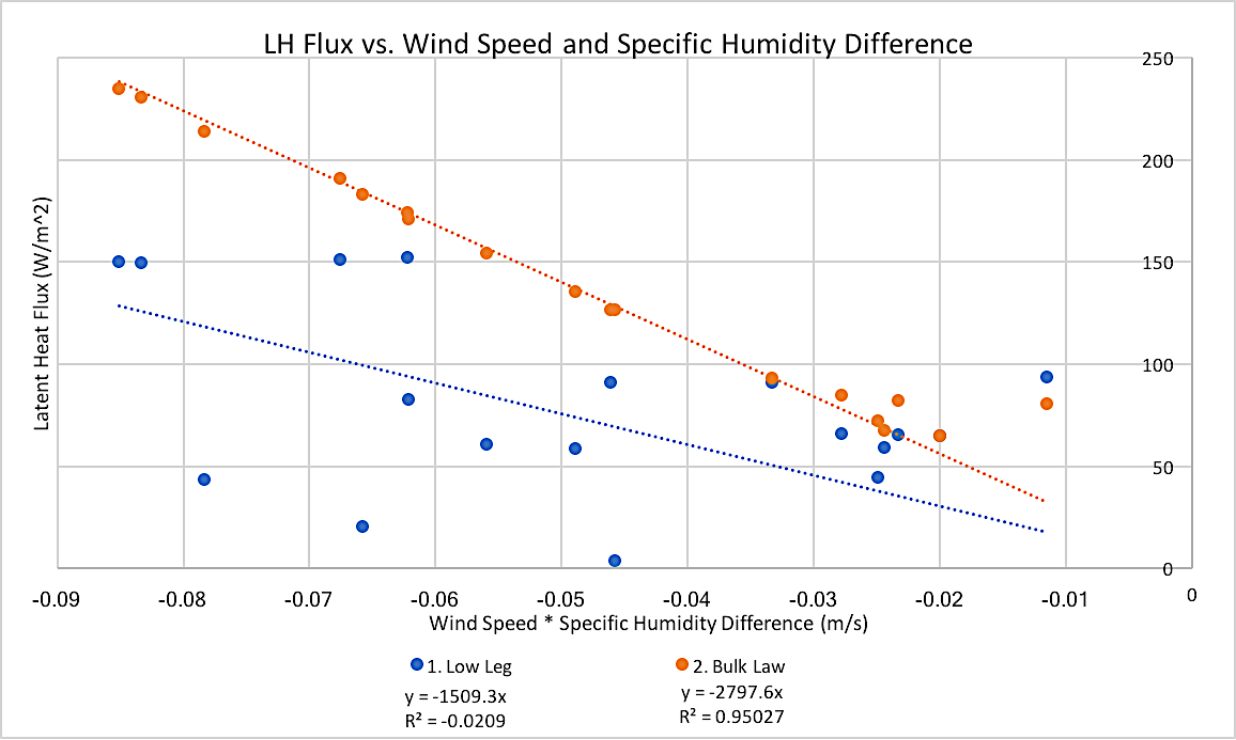

Figure 4.3.2. Latent Heat Flux and the product of the wind speed and the specific humidity difference at the surface. Method 1 (Flight level flux) is shown in blue, and Method 2 (Bulk Law) is shown in orange. Fits are linear and through the origin.

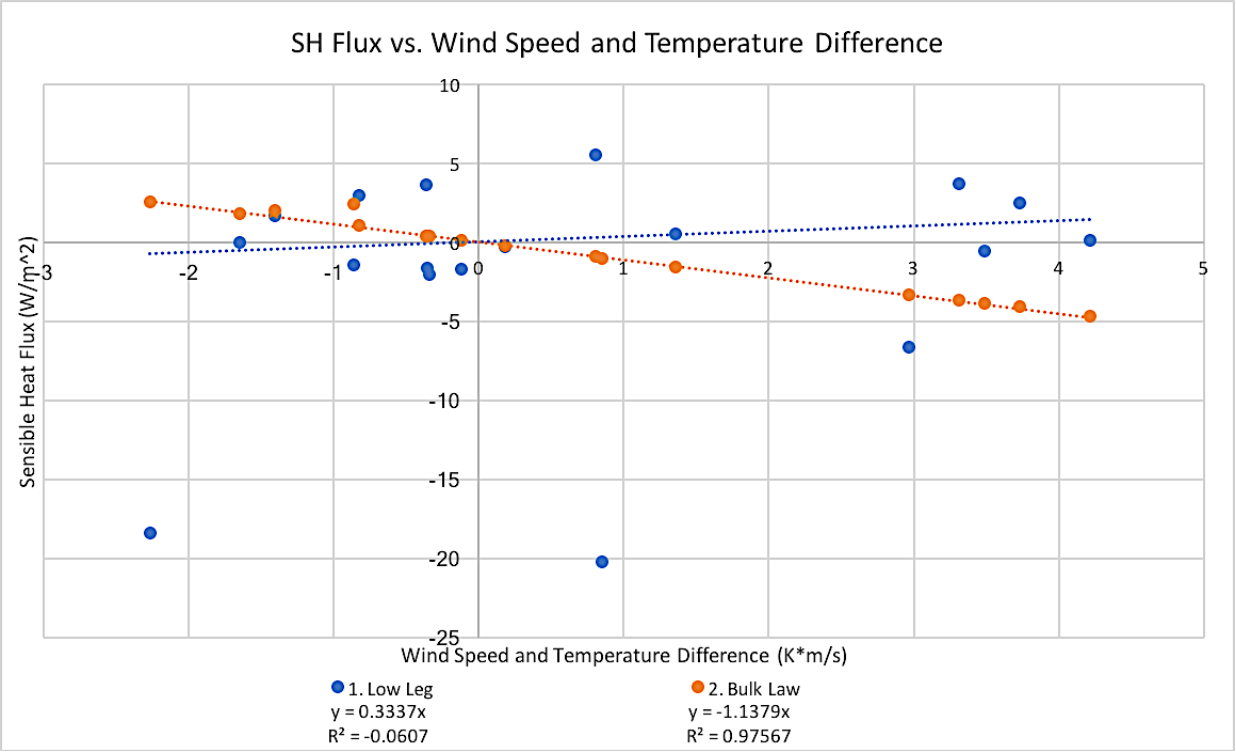

Figure 4.3.3. Sensible Heat Flux and the product of the wind speed and the temperature difference at the surface. Method 1 (Flight level flux) is shown in blue, and Method 2 (Bulk Law) is shown in orange. Fits are linear and through the origin.

4.4. Summary of Results

LES models produces vertical profiles of each flux examined in this section, and allows for comparison to the vertical variation in the fluxes from aircraft measurements. The fluxes generated from aircraft data do not reflect the variability suggested in the vertical profiles generated by large eddy simulation models, particularly in the sub-cloud layer, at the surface and the 300m flight level. The constant values for latent heat flux in the sub-cloud layer expected by LES models are not confirmed in the aircraft data. On the other hand, the variations in sensible heat flux, changing sign in the sub-cloud layer, are reflected in the aircraft data. While the aircraft momentum fluxes are quite small, like the LES models, the strong decrease in momentum flux through the sub-cloud layer is not reflected by aircraft data.

In comparing the aircraft fluxes at 1200m, 300m, and the surface, there is no correlation between fluxes at the high flight level and the low flight level. This is likely due to the presence of the lifted condensation level and the cumulus cloud layer between the two flight levels. On the other hand, there is correlation between the sensitivities of the low flight level fluxes and the surface fluxes in the zonal momentum flux. Wind speed exhibits the strongest sensitivities in comparing the surface fluxes and the low flight level fluxes; however, wind speed does not correlate with any fluxes in the high flight level.

5. Results/Comparison of ERA5 and Aircraft Fluxes

5.1. Comparison of atmospheric variables

To better understand the correlations and discrepancies between the aircraft data and the ERA5 model, the quantities that are used in the bulk laws are compared: 10m wind speed (U), sea surface temperature (SST), surface air temperature (T_{2m}), specific humidity at saturation (q_{sat}), and surface specific humidity (q). Then the resulting surface flux values are compared. The methods of computing fluxes and average values are summarized in Table 5.1.1.

Two methods of calculating flux values use aircraft measurements: the first is direct measurements at flight level based on eddy correlation method (Flux Method 1), and the second is calculating fluxes with the bulk law using aircraft measurement values (Flux Method 2). The other two methods are through ERA5 reanalysis: the third is the values of

surface flux as calculated by the ERA5 model parameterizations (Flux Method 3), and the fourth is calculating fluxes with the bulk law using ERA5 model values for atmospheric variables (Flux Method 4).

	Latent Heat Flux	Mean Value (W/m^2)	Sensible Heat Flux	Mean Value (W/m^2)	Momentum Flux	Mean Value (N/m^2)
Method 1	$LHF = \rho L \overline{w'q'}$	80.488	$SHF = \rho c_p \overline{w'\theta'}$	12.719	$UMF=\rho \overline{w'u'}$ $VMF=\rho \overline{w'v'}$	UMF= 0.03768
Method 2	$LHF = \rho L C_L U \Delta q$	138.16	$SHF = \rho c_p C_S U \Delta T$	-0.67787	$UMF = \rho C u^2$ $VMF = \rho C v^2$	UMF= 0.03624
Method 3	$LHF = \rho L C_Q U \Delta q$	131.42	$SHF = \rho c_p C_H U \Delta T$	8.2299	$UMF = \rho C u^2$ $VMF = \rho C v^2$	UMF= 0.0826
Method 4	$LHF = \rho L C_L U \Delta q$	175.32	$SHF = \rho c_p C_S U \Delta T$	-1.8038	$UMF = \rho C u^2$ $VMF = \rho C v^2$	UMF= 0.04283

Table 5.1.1. Summary of Flux Calculation Methods (Refer to Section 3)

The 10-meter wind speed value is a key variable in all three surface fluxes. Figure 5.1.2 compares the 10m wind speed (U) values from the aircraft data (calculated by the power law in Eqn. 18) and from the ERA5 model. There is a very close correlation, with a linear fit of $y = 1.0209\,x + 1.4067$ m s^{-1}, and R^2=0.77899. With a small offset, there is a nearly one-to-one correlation between the sets (one-to-one line shown in orange). In the 2011 paper, "TropFlux: air-sea fluxes for the global tropical oceans—description and evaluation," Kumar, et al. find that ERA5 has a negative bias in wind speed in comparison to other reanalysis products. This is not consistent with the comparison to the aircraft measurements. This should result in consistent momentum flux values.

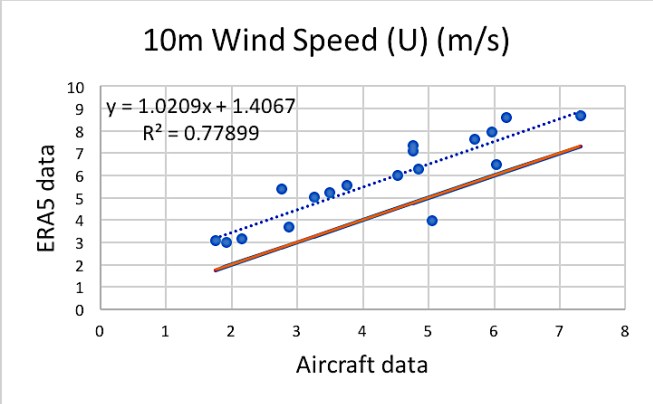

Figure 5.1.2. 10-Meter Wind Speed from aircraft data and ERA5 model. The linear regression is shown with the blue dotted line (and equation given) and a one-to-one correlation is shown with the orange line.

Figure 5.1.3 compares the values for surface specific humidity (q) from aircraft measurement and the ERA5 model, and Figure 5.1.4 compares the values for specific humidity at saturation (q_{sat}). There are moderate correlations between the aircraft data and the ERA5 model for both q and q_{sat}, and for the difference between the two values, plotted with a linear fit of $y = 0.514\ x + 0.0047$ (kg/kg), and a correlation of $R^2 = 0.69532$ (Figure 5.1.5). The range of values is greater in the aircraft data, indicating that the aircraft measures greater range in day-to-day variations than the model. Also, average values for Δq from the aircraft is around 0.007 kg/kg, but is higher from the ERA5 model, around 0.009 kg/kg.

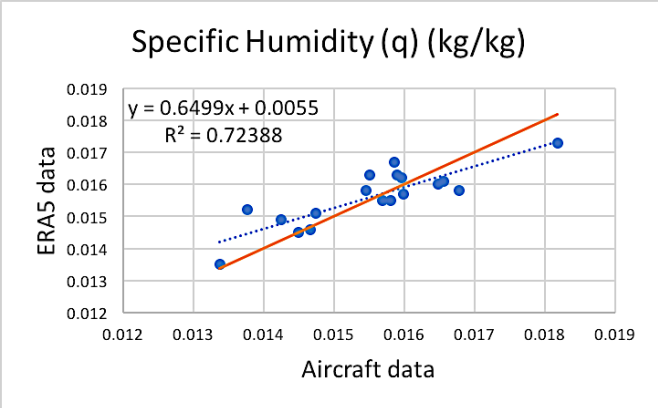

Figure 5.1.3. Specific Humidity at the surface from aircraft data and ERA5 model.

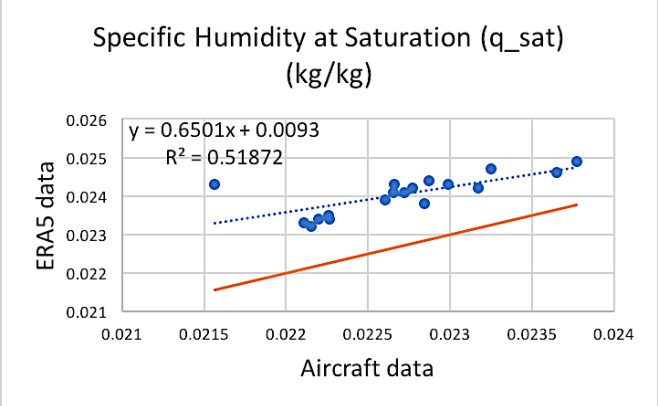

Figure 5.1.4. Specific Humidity at Saturation at the surface from aircraft data and ERA5 model.

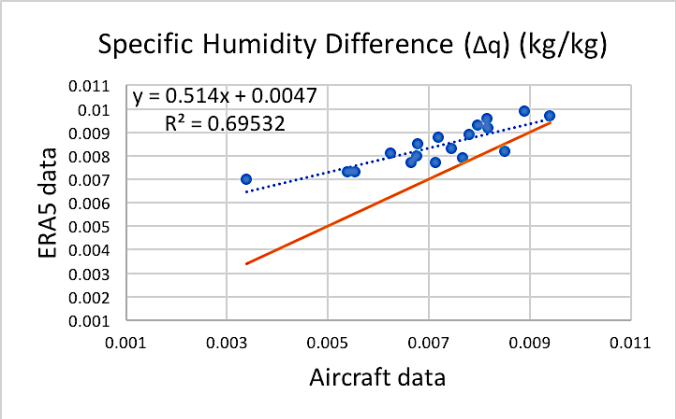

Figure 5.1.5. Specific Humidity difference at the surface from aircraft data and ERA5 model. Note the greater range of values from the aircraft measurements.

Figure 5.1.6 shows a comparison of sea surface temperature (SST) values for aircraft measurements and ERA5 model. The linear fit for the data has an equation of $y = 0.5867x + 124.12$ K, and a moderate correlation with $R^2=0.47863$. The aircraft measurements exhibit a greater range of values reflecting a greater daily variation in SST; however, the average values of SST for both datasets are close. There is significantly less correlation in the temperature for two meters above the sea surface, as shown in Figure 5.1.7. There is a much greater range in air temperature values from the aircraft data, and the ERA5 values for air temperature are on average lower than the aircraft values by nearly 1K. The aircraft values are calculated from the dry adiabatic lapse rate, which may introduce error; however, Kumar, et al. find a similar bias in the ERA5 temperature variables in comparison to other reanalysis models (such as NCEP and NCEP2).

The lack of correlation in the 2-meter air temperature is reflected in the temperature difference between the surface and the air above, ΔT (Eqn. 14). The values for ΔT are systematically greater in the ERA5 model than as calculated from the aircraft measurements (as shown in Figure 5.1.8). While the aircraft data produces some negative values ($T_{air}>SST$), the ERA5 model produces no downward flux values.

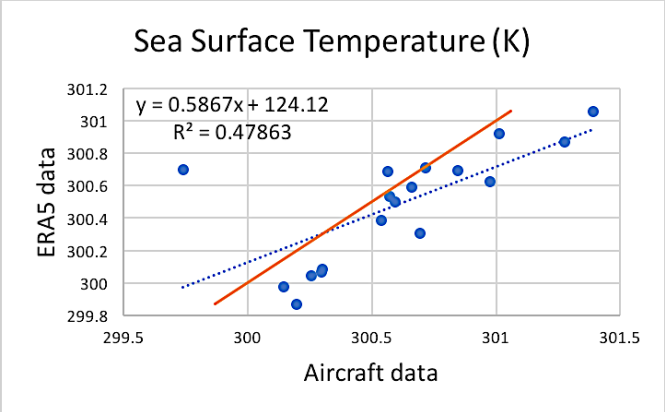

Figure 5.1.6. Sea Surface Temperature from Aircraft data and ERA5 model.

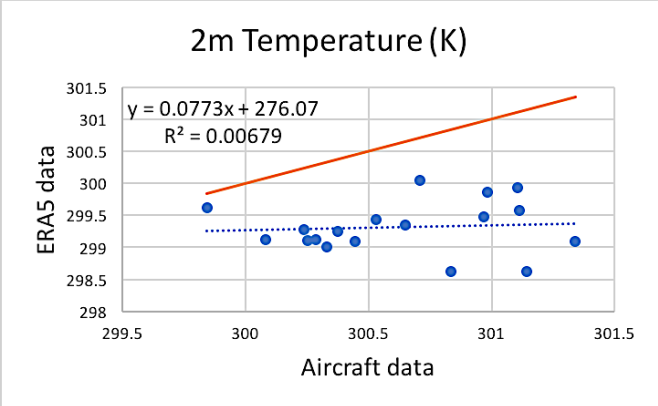

Figure 5.1.7. Air Temperature 2 meters above the surface calculated from aircraft data and modelled by ERA5. Note the lesser values from the ERA5 model.

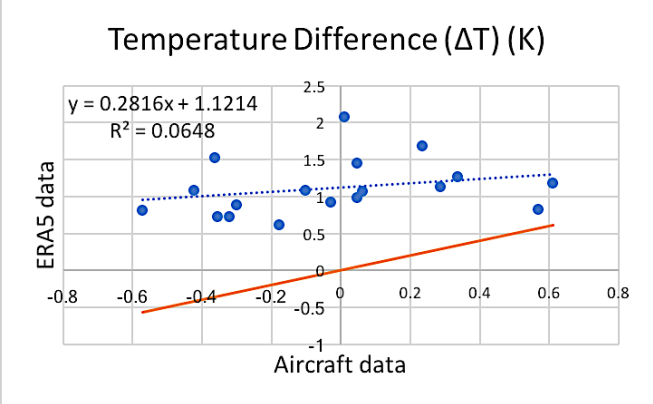

Figure 5.1.8. Temperature difference between the sea surface and the air 2m above the surface, calculated from aircraft data and modelled by ERA5. Note the greater values of the ERA5 model.

5.2. Comparison of Aircraft fluxes and ERA5 fluxes

This section will directly compare results from the four methods of calculating fluxes in order to evaluate the various methods of calculations and the effect of the discrepancies in atmospheric variables as discussed in Section 5.1.

Figure 5.2.1 shows latent heat flux as calculated by Method 3 and Method 4, both of which use ERA5 atmospheric conditions. Method 4 systematically results in higher latent heat flux values. Given that Method 3 and Method 4 differ only in the bulk transfer coefficients, this result indicates that the empirical value of $C_Q = 1.2x10^{-3}$ (Stewart, 2008) is systematically greater than the of Monin-Obukhov similarity theory in the ERA5 model.

In Figure 5.2.2, the discrepancies of Figure 5.2.1 are compounded by comparing Method 2 (bulk laws with aircraft data) to Method 3 (ERA5 parameterization). The linear fit shows a weaker, but overall moderate correlation between the two datasets, with R^2=0.76583. While these discrepancies are more difficult to isolate, the graph shows that Method 3 yields higher values that Method 2 on low flux days, but lower values than Method 2 on high flux days. In other words, the aircraft produces greater daily variation in latent heat fluxes at the surface.

Comparing Method 2 and Method 4 is an extension of Section 5.1, because Method 2 and Method 4 differ only in values of atmospheric conditions. Figure 5.2.3 compares Methods 2 and 4, and reflects systematically larger values from Method 4, consistent with the results of Figure 5.1.5, in which ERA5 also yielded larger values of Δq.

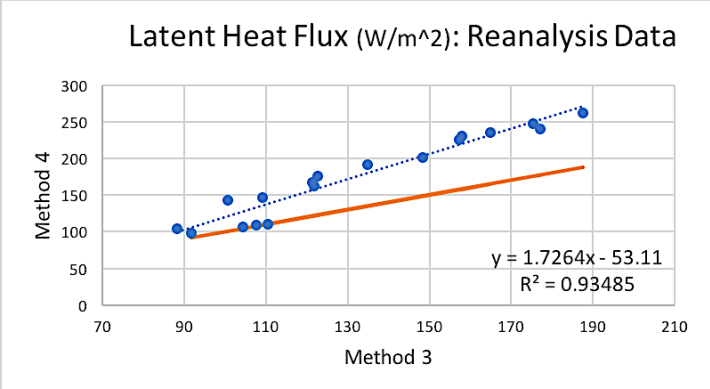

Figure 5.2.1. Latent Heat Flux: Comparison of Method 3 and Method 4.

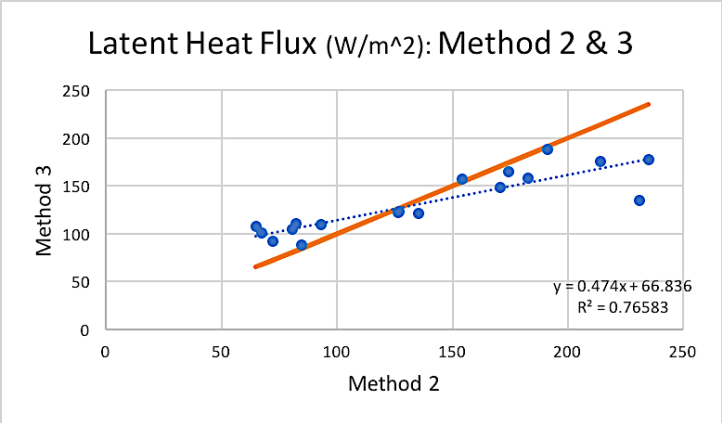

Figure 5.2.2. Latent Heat Flux: Comparison of Method 2 and Method 3.

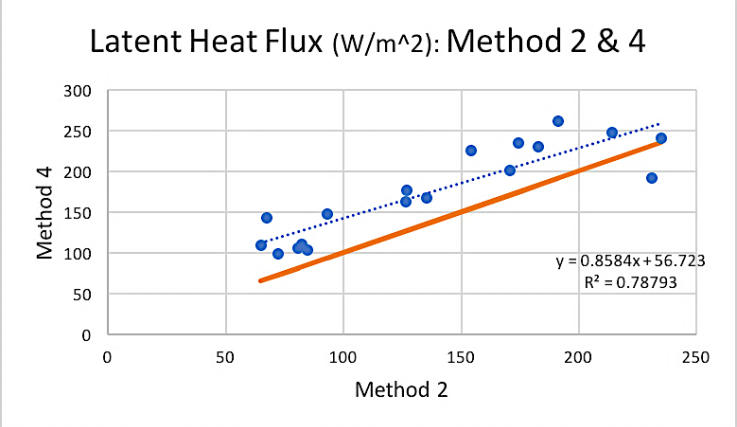

Figure 5.2.3. Latent Heat Flux: Comparison of Method 2 and Method 4.

Sensible heat flux calculations are similarly compared in Figures 5.2.4-6. In comparing the two sets of ERA5 determined fluxes, Figure 5.2.4 shows that the bulk law with the empirically determined constant ($C_H = 1.0x10^{-3}$) is generally less than the coefficient as determined the ERA5 parameters. While the coefficient also accounted for discrepancies in the latent heat fluxes, it was of the opposite sign. C_H, as determined by the ERA5 model, is greater than the empirical value. There is a much weaker correlation between the Method 2 and Method 3 (Figure 5.2.5). Method 3 (ERA5 parameterizations) are all positive values, whereas Method 2 (aircraft bulk laws) yields negative fluxes. Method 3 also calculates higher flux values over a larger range. Comparing Method 4 to Method 2 (Figure 5.2.6) reflects the same discrepancies between the aircraft ΔT values and the reanalysis ΔT values. These results reflect the systematically higher ΔT values produced from reanalysis data.

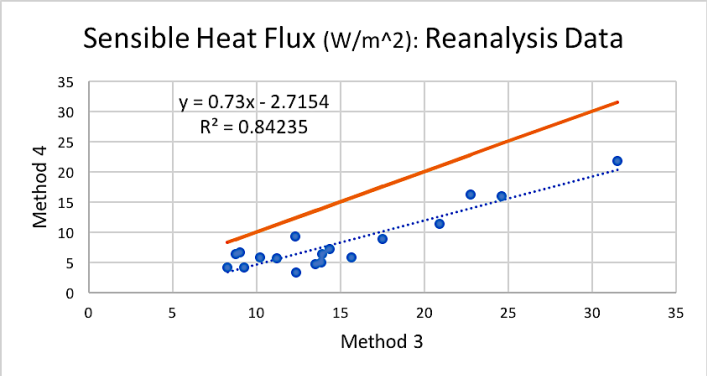

Figure 5.2.4. Sensible Heat Flux: Comparison of Method 3 and Method 4 (reanalysis methods).

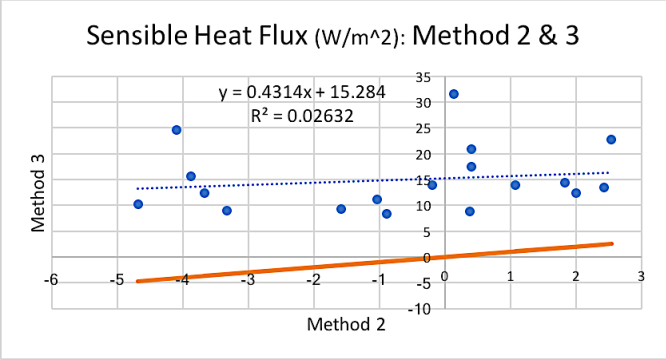

Figure 5.2.5. Sensible Heat Flux: Comparison of Method 2 and Method 3.

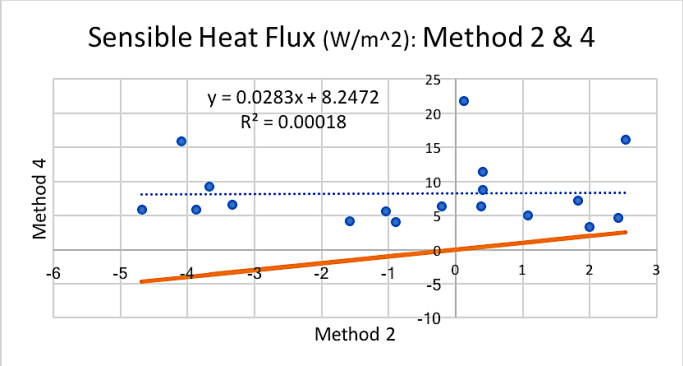

Figure 5.2.6. Sensible Heat Flux: Comparison of Method 2 and Method 3. Compare to Figure 5.1.8, which shows values of ΔT.

Figure 5.2.7 shows the zonal momentum flux calculated with Method 3 and Method 4, the two methods that use reanalysis variables. While there is a moderate correlation between the two sets, it is not a one-to-one correlation. Method 4 yields lower values while Method 3 yields a greater range of values, likely because of the parameterization of the drag coefficient (C_D). The drag coefficient in Method 4 is constant, whereas the drag coefficient in

Method 3 is a function of wind speed, and therefore is greater at higher wind speeds, resulting in a greater range of values in the resulting momentum flux. The trends in Figure 5.2.9. are a result of the same discrepancies in wind stress coefficients as in Figure 5.2.7, because Method 4 and Method 2 both use the empirical wind stress coefficient constant value of $1x10^{-3}$. High wind schemes ($U>6$ m s^{-1}) for wind stress coefficients are offered by Garratt (1977) or Smith (1980).

Given the strong correlations between aircraft and reanalysis wind speed values, I expect strong correlations in aircraft and reanalysis values for momentum flux. This is true for zonal momentum fluxes; however, the meridional momentum fluxes are occasionally zero and show greater scatter over smaller range. The correlation between Method 2 and Method 4 (Figure 5.2.8) reflects the correlation in 10m wind speed values determined by ERA5 model and aircraft data (figure 5.1.2). Momentum flux depends on U^2 in Method 2 and Method 4, so those methods never produce negative fluxes.

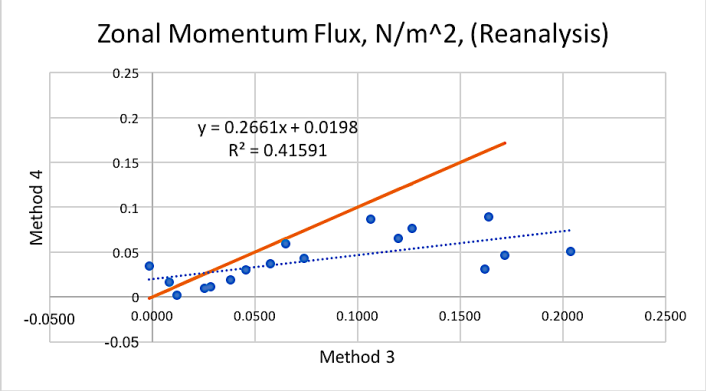

Figure 5.2.7. Zonal Momentum Flux Comparison of Method 3 and Method 4 (Reanalysis methods).

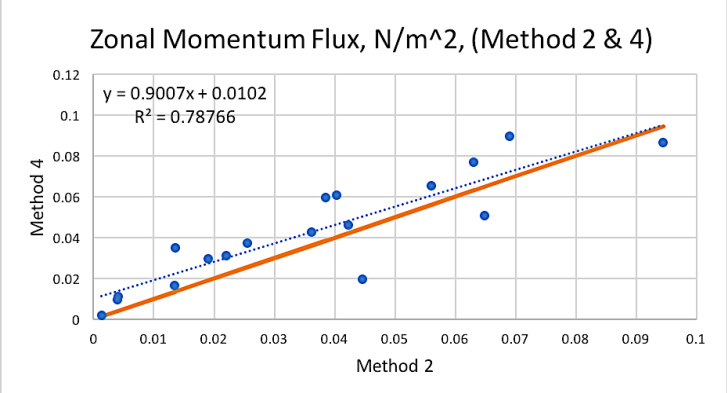

Figure 5.2.8. Zonal Momentum Flux: Comparison of Method 2 and Method 4 (Bulk law methods).

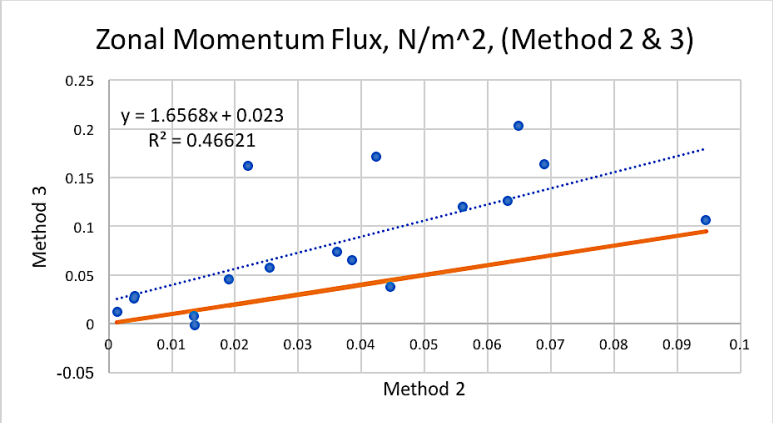

Figure 5.2.9. Zonal Momentum Flux: Comparison of Method 2 and Method 3.

5.3. Summary of Results

In comparing results of the ERA5 reanalysis model and data measured by the aircraft, there is a strong correlation between wind speed values. However, ERA5 reanalysis produces larger values for specific humidity at saturation, and smaller values for air temperature at 2 meters, resulting greater Δq and ΔT values at the surface. This leads to discrepancies in the flux values for latent heat and sensible heat.

Discrepancies are also caused by the different definitions of the transfer coefficients in the bulk laws in ERA5 reanalysis values for fluxes and the bulk law values. ERA5 defines the transfer coefficients with profile functions and Monin-Obukhov boundary layer theory, altering the coefficients in iterative calculations, while the bulk law of Method 4 use constant values for transfer coefficients defined empirically. Comparison of the flux values calculated from Method 3 and Method 4 indicates that the empirical constant transfer coefficient for latent heat is greater and the constant transfer coefficient for sensible heat is less than the coefficients determined by ERA5 parameterizations. The empirical wind stress coefficient is constant because of the lack of high wind days ($U>6$ m s^{-1}), but the ERA5 parameterizations yield a greater range of high momentum flux values, consistent with a high-wind scheme for calculating the drag coefficient.

6. Tropical Fluxes in Global Climate

6.1. Regional Comparison

The data provided from DOMEX research flights span a small region of the western tropical Atlantic. To determine how this area is unique, and how it fits into a global perspective of air-sea fluxes, ERA5 model fluxes from the western tropical Atlantic are compared to 4 other tropical regions of global oceans. Table 6.1.1 summarizes the comparison. While the trade winds are expected to be the prevailing winds (u) in each region, they are strongest over the eastern Pacific and the central Indian Ocean, weaker in the western Pacific and western Atlantic regions, and nearly absent in the eastern Atlantic region. The specific humidity (q) at the surface does not vary greatly by region.

Sea surface temperature varies remarkably by region. In particular, the SST values for the regions on eastern boundaries of ocean basins are lower than the regions on the western boundaries by 5K or more. This is consistent with the dynamics of ocean gyres, in which the eastern boundary currents transport cold water from pole to equator and the western boundary currents transport warm water from equator to pole. In the Atlantic, the lower SST in the east is matched by lower sensible heat fluxes and latent heat fluxes; however, the trend is not present in the Pacific.

The Bowen ratio, that is, the ratio of sensible heat flux to latent heat flux is useful to compare the latent heat fluxes and sensible heat fluxes among regions. The Bowen Ratio is positive and less than one for all 5 regions, indicating that latent heat flux and sensible heat flux are both positive, and latent heat flux is the larger quantity. However, the Bowen ratio is an order of magnitude smaller in the eastern Atlantic in comparison to the other regions, and the Western Atlantic, exhibits the greatest value for the Bowen ratio. In general, flux values from the Western Atlantic are fairly consistent with values from the Pacific and Indian ocean regions, but not consistent with the eastern Atlantic region.

Region	Western Atlantic	Eastern Atlantic	Western Pacific	Eastern Pacific	Indian Ocean
Latitude	14-16ºN	14-16ºN	14-16ºS	14-16ºS	14-16ºS
Longitude	60-62ºW	19-21ºW	168-170ºW	98-100ºW	68-70ºE
u at 10m (m/s)	-5.422	0.214	-4.781	-7.000	-7.841
SST (K)	300.360	293.910	302.112	297.616	300.365
q (kg/kg)	0.015	0.012	0.017	0.012	0.015
LHF (W/m^2)	137.215	54.956	128.943	157.208	176.746
SHF (W/m^2)	13.918	0.075	12.254	11.830	12.185
Bowen Ratio	0.101	0.001	0.095	0.075	0.069
UMF (N/m^2)	0.076	0.000	0.040	0.089	0.114
VMF (N/m^2)	0.017	0.089	0.001	0.034	0.038

Table 6.1.1. Regional Comparison: Mean conditions and surface fluxes for April 2011.

6.2. Seasonal Cycle of Air-Sea Fluxes

The seasonal cycles of air-sea fluxes in the tropics, outside of the measurement window of the DOMEX project, are important for understanding these findings in a climatological context. While diurnal cycles also cause variations in these fluxes, this analysis focuses on seasonal cycles of the atmospheric conditions and the resulting fluxes. ERA5 model is run for monthly averages of surface fluxes and atmospheric conditions for the years 2000-2019 over the western tropical Atlantic region.

Specific humidity at the surface demonstrates a maximum in the summer months and a minimum in the winter months. This is consistent with the seasonal cycle of air temperature, as the Clausius-Clapeyron relation states that warmer air holds more water vapor. Figure 6.2.1 shows the monthly average values for surface latent heat flux. The flux is at a minimum in the summer months when specific humidity is highest, and is maximum in the winter months when specific humidity is lowest. Therefore, the data in this study (in April and May) captures a period between a maximum and a minimum.

Sea Surface Temperature exhibits a strong maximum in the late summer (September) and a minimum in late winter (March), due to the seasonal fluctuations of solar radiation in the tropics. Figure 6.2.2 shows the monthly average values of surface sensible heat flux. Sensible heat flux is generally higher in the winter months than the summer months. The data in this study, therefore, captures a period between a maximum and a minimum in sensible heat flux.

Zonal momentum flux follows the seasonal cycle of the zonal winds (the easterly trade winds). Figure 6.2.3 demonstrates this cycle, in which wind speed and momentum flux are at a maximum in winter, and also have a peak in summer. Therefore, the DOMEX data includes a minimum in the seasonal cycle of trade wind strength and zonal momentum flux.

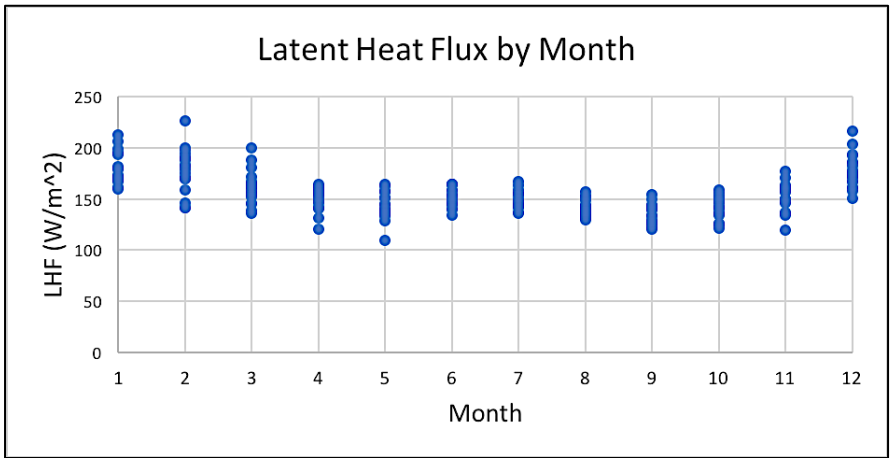

Figure 6.2.1. Latent Heat Flux: Seasonal Cycle. ERA5 monthly averages for 2000-2019.

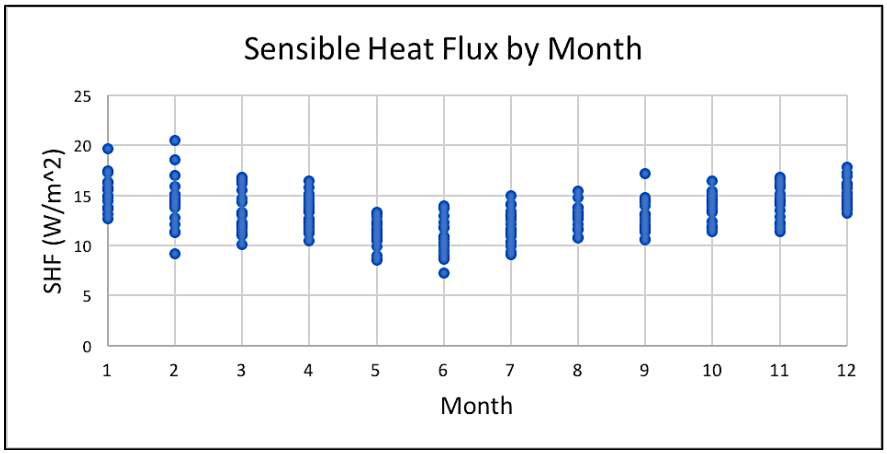

Figure 6.2.2. Sensible Heat Flux: Seasonal Cycle. ERA5 monthly averages for 2000-2019

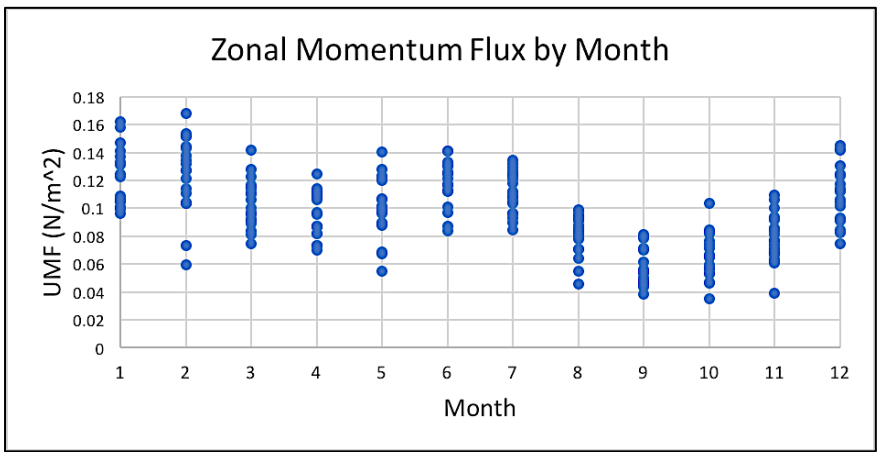

Figure 6.2.3. Momentum Flux: Seasonal Cycle. ERA5 monthly averages for 2000-2019

7. Conclusion

This study compares four methods of flux calculations, and evaluates the results from two datasets. Using aircraft data from the DOMEX project, latent heat flux, sensible heat flux, and momentum flux are calculated at flight level by eddy correlation method and at the surface by the bulk law. These results agreed reasonably well with vertical profiles of fluxes determined by large eddy simulation models (Siebesma et al., 2003).

Aircraft measurements of fluxes in future studies could be improved with flights at more levels and longer flight lengths, in order to better evaluate flux profiles and decrease eddy correlation method uncertainties. As determined by Lenschow, et al. (1993), 90km flight legs are necessary for minimal error in aircraft measurements of fluxes by eddy correlation. Flights at more vertical levels would increase vertical resolution of fluxes and offer a better understanding of how these fluxes change with height, especially in the boundary layer, and in strong convection scenarios. Furthermore, as the results of Section 6.1 show, there is variation in air-sea fluxes across ocean basins. Conducting aircraft measurement field campaigns in locations across an ocean basin would provide data to investigate regional variation in fluxes, within and beyond the tropics. Flux sensitivities to wind speed, temperature, and moisture above the surface, would be also be better studied with measurements of fluxes throughout the seasonal cycle, to measure fluxes through a variety of atmospheric conditions.

The aircraft fluxes were compared to ERA5 reanalysis model values for mean atmospheric conditions and surface fluxes. The flux calculations that used empirically determined coefficients of bulk transfer were not consistent with the ERA5 model parameterizations, which employed Monin-Obukhov similarity theory. In comparison to aircraft measurements, the ERA5 model did not fully capture day-to-day variation in mean atmospheric conditions. Furthermore, the model exhibited biases in specific humidity at saturation and 2-meter air temperature, affecting the model's values for surface fluxes.

The model's biases in air temperature and specific humidity conditions result in biases in surface flux values. The high surface flux values impact the results of climate models in local thermodynamic processes like convection and in large-scale imbalances in the

surface energy budget. Specifically, the heat flux values produced by the model would affect short-term phenomena like cloud formation or model increased severity of tropical cyclones. Higher sensible heat flux values would have an impact on global circulation models in which the tropics serve as a heat engine, and in local cumulus convection in the tropics.

Acknowledgements

Thank you to Professor Smith for supervising this project. Your patient guidance and insights throughout this project were immensely helpful. Thank you to Professor Fedorov for acting as a reader as well. I am also grateful for the help of Professor Alison Nugent in her help to get MatLab codes up and running. Finally, I am thankful for the support of the Geology & Geophysics department at Yale throughout this project and over the last four years.

Appendix

Data from DOMEX

Variable	Name in Dataset	Measurement Instrument
Temperature (C)	'trf'	reverse-flow temperature sensor
Surface Temperature (C)	'rstb'	Infrared radiometer
Dry Potential Temperature (C)	'thetad'	Calculated from temperature and pressure measurements
Water Vapor Mixing Ratio (g/kg)	'mr'	Chilled Mirror Sensor
Altitude (m)	'ralt1'	Radio Altimeter
Pressure (millibar)	'ps_hads_a'	Rosemont Digital Sensor
Pressure (Pa)	'licorp'	LICOR Gas Analyzer
Wind Speed	'hu', 'hv', 'hw'	Applanix Instrument

Calculated Variables:

Variable	Formula	Constants/Data	Assumptions
Surface Pressure	$P_{surf} = P(z) - (\rho * g * z)$	$\rho = 1.2 kg/m^2$ P(z) = P at altitude Z = flight altitude	Hydrostatic Balance
Surface Temperature	$T_{air} = T(z) + g(z/10^3)$	T = T at altitude	Dry Adiabatic Lapse Rate = g=9.81K/km
Saturation Vapor Pressure	e_s = polynomial approx. of Clausius-Clapeyron Relation	SST = Sea Surface Temperature	Reference: Lowe, 1976
Saturation Mixing Ratio	$mrsat = \frac{0.662 * e_s}{P - e_s}$		Reference: Marshall & Plumb, 2008
Specific Humidity	$q_{sat} = \frac{mr_{sat}}{1 + mr_{sat}}$ $q_{air} = \frac{mr_{air}}{1 + mr_{air}}$		Reference: AMS Glossary of Meteorology
Ten Meter Wind Speed	$u_{10m} = \frac{u(z)}{\left(\frac{z}{10}\right)^{\frac{1}{7}}}$	u(z) = wind speed at Altitude	Power Law for Fluid Flow at a boundary

From Lowe, 1976: $e_s = a_0 + T(a_1 + T(a_2 + T(a_3 + T(a_4 + T(a_5 + a_6 T)$

$a_0 = 6984.505294$;
$a_1 = -188.9039310$;
$a_2 = 2.133357675$;
$a_3 = -1.288580973 \times 10^{-2}$;
$a_4 = 4.393587233 \times 10^{-5}$;
$a_5 = -8.023923082 \times 10^{-8}$;
$a_6 = 6.136820929 \times 10^{-11}$

Constants:

Constants	Value	Reference
Latent Heat Transfer Coefficient	$C_L = 1.2x10^{-3}$	Stewart, 2008
Sensible Heat Transfer Coefficient	$C_S = 1x10^{-3}$	Stewart, 2008
Momentum Transfer Coefficient	$C_D = 1x10^{-3}$	Sahlee, 2008

References Cited

Augstein, E., H. Schmidt, and F. Ostapoff, 1974: The vertical structure of the atmospheric planetary boundary layer in undisturbed trade winds over the Atlantic Ocean. *Boundary-Layer Meteorology.* 6: 129–150.

Beljaars, A.C.M., 1997: Air-Sea Interaction in the ECMWF Model. In Proc. of ECMWF Seminar on Atmosphere Surface Interaction. 33–52.

Betts, A.K., R.L. Desjardins, J.I. MacPherson, et al., 1990: Boundary-Layer Heat and Moisture Budgets from FIFE. *Boundary Layer Meteorology.* 50: 109-137.

Copernicus Climate Change Service (C3S) (2017): ERA5: Fifth generation of ECMWF atmospheric reanalyses of the global climate. Copernicus Climate Change Service Climate Data Store (CDS), April 18, 2020. https://cds.climate.copernicus.eu/cdsapp#!/home

Deardorff, J.W., 1968: Dependence of Air-Sea Transfer Coefficients on Bulk Stability. *Journal of Geophysical Research*. 73(8): 2549-2557.

Dunckel, M., L. Hasse, L. Krügermeyer, et al., 1974: Turbulent fluxes of momentum, heat and water vapor in the atmospheric surface layer at sea during ATEX. *Boundary-Layer Meteorology*. 6: 81–106.

Garratt, J.R., 1977: Review of Drag Coefficients over Oceans and Continents. *Monthly Weather Review*. 105: 915-929.

Gill, A. E., 1982: *Atmosphere- Ocean Dynamics*. Academic Press.

Haiden, T., 1996: An Analytical Study of Cumulus Onset. Quarterly Journal of the Royal Meteorological Society. 123: 1945-1960.

Hersbach, H., B. Bell, P. Berrisford, et al., 2019: Global Reanalysis: Goodbye ERA-Interim, Hellow ERA5. ECMWF Newsletter. 159: 17-24.

Hoeber, H., 1974: The Boundary-Layer Subprogram for GATE. *Bulletin of American Meteorological Society*. 55(7): 731-734.

Holland, J.Z., 1972: Comparative Evaluation of Some BOMEX Measurements of Sea Surface Evaporation, Energy Flux and Stress. *Journal of Physical Oceanography.* 2: 476–486.

Holtslag, A.A.M., and H.A.R. DeBruin, 1988: Applied Modeling of the Nighttime Surface Energy Balance over land. Journal of Applied Meteorology. 27: 689-704.

IFS Documentation CY46R1: Part IV Physical Processes. European Center for Mid-Range Weather Forecasts. 2019.

Knauss, J. A. and N. Garfield, 2017: *Introduction to Physical Oceanography: Third Edition*. Waveland Press.

Kuettner, J. P., 1974: General Description and Central Program of GATE. *Bulletin of American Meteorological Society*. 55(7): 712-719.

Kumar, B.P., J. Vialard, M. Lengaigne, et al., 2012: TropFlux: Air-Sea Fluxes for the Global Tropical Oceans—Description and Evaluation. *Climate Dynamics*. 38: 1521–1543.

Kundu, P. K. and Cohen, I. M., 2002: *Fluid Mechanics*. Academic Press.

Kuettner, J. P. and J. Holland, 1969: The BOMEX Project. *Bulletin of American Meteorological Society*. 50(6): 394-402.

Lawrence, M.G., 2005: The Relationship between Relative Humidity and the Dewpoint Temperature in Moist Air. *Bulletin of the American Meteorological Society*. 86: 225–234.

Lee, X., 2018: *Fundamentals of Boundary-Layer Meteorology*. Springer.

LeMone, M.A., W.M. Angevine, C.S. Bretherton, et al., 2019: 100 Years of Progress in Boundary Layer Meteorology. *Meteorological Monographs.* 59: 9.1–9.85.

Lenschow, D.H., J. Mann, and L. Kristensen, 1993: How Long is Long Enough When Measuring Fluxes and Other Turbulent Statistics? Journal of Atmospheric and Oceanic Technology. 11, 661-673.

Lowe, P.R., 1976: An Approximating Polynomial for the Computation of Saturation Vapor Pressure. *Journal of Applied Meteorology*. 10: 101-103.

Paulson, C.A., E. Leavitt, and R.G. Fleagle, 1972: Air-Sea Transfer of Momentum, Heat and Water Determined from Profile Measurements During BOMEX. *Journal of Physical Oceanography.* 2: 487–497.

Sahlée, E., A. Smedman, U. Högstöm, et al., 2008: Reevaluation of the Bulk Exchange Coefficient for Humidity at Sea during Unstable and Neutral Conditions. Journal of Physical Oceanography. 38: 257-272.

Siebesma, A.P., C.S. Bretherton, A. Brown, et al., 2003: A Large Eddy Simulation Intercomparison Study of Shallow Cumulus Convection. Journal of Atmospheric Sciences. 60(10):1201-1219.

Siebesma, A.P., and J.W.M. Cuijpers,1994: Evaluation of Parametric Assumptions for Shallow Cumulus Convection. Journal of Atmospheric Sciences. 52(6): 650-666.

Smith, S.D., 1980: Wind Stress and Heat Flux over the Ocean in Gale Force Winds. *Journal of Physical Oceanography*. 10: 709-726.

Smith, S.D., 1988: Surface Wind Stress, Heat Flux, and Wind Profiles as a Function of Wind Speed and Temperature. *Journal of Geophysical Research*. 93(C12): 15467-15472.

Smith, R.B., J.R. Minder, A.D. Nugent, et al., 2012: Orographic Precipitation in the Tropics: The Domenica Experiment. *Bulletin of American Meteorological Society*. 93: 1567-1579.

Stewart, R.H., 2008: *Introduction to Physical Oceanography*. Texas A & M University.

Stull, R. B., 1988: *An Introduction to Boundary Layer Meteorology*. Kluwer Academic Publishers.

Thompson, N., K.L. Webber, and B.P. Norris, 1980: Eddy-fluxes and spectra in the GATE sub-cloud layer. *Quarterly Journal of the Royal Meteorological Society*. 106: 277-292.